*Tellus (1996), 48A, 238–253*
*Printed in Belgium – all rights reserved*



**TELLUS**
*ISSN 0280–6495*

# Low-frequency oscillations and associated wave motions over Eurasia

By XIAOLAN WANG*, JOÃO CORTE-REAL and XUEBIN ZHANG, *Department of Physics, Faculty of Sciences, University of Lisbon, Campo Grande, Ed. C1, Piso 4, 1700 Lisbon, Portugal*

(Manuscript received 31 May 1994; in final form 6 June 1995)

ABSTRACT

Based on 5-day-mean grid point data for both 500-hPa geopotential height (Z500) and sea level pressure (SLP) fields, and focusing on periods of 4 weeks to a year, surface and mid-tropospheric low-frequency oscillations over Eurasia are extracted by using multi-channel singular spectrum analysis (MCSSA), combined with the maximum entropy method. Besides the permanent annual cycle (365 $\sim$ 366 days) and its second harmonic (181 days), low-frequency oscillations with periods of 55–65 and 35–45 days were found both in the mid-troposphere and at sea level, explaining a substantial number of the total variances in the relevant frequency bands. These quasi-periodicities are robust, since they are reproducible when different window lengths are used and when MCSSA is applied to two equal-length subsets of the basic data series, and since they are qualitatively different from those obtained from randomly resampled basic datasets. Moreover, no periodicities were reproduced from scrambled basic datasets. The spatial-temporal structures of these low-frequency oscillations, i.e., the associated wave motions, are presented, in order to display evolutionary processes of circulation systems probably related to the Asian monsoon variability. Some reliable information about the amplitudes of the oscillations is also obtained by using composite analysis. The 55–65 day oscillation is, in the mid-troposphere, associated with transitions between flow regimes of intense anomalies over the polar cap-Ural mountains, matched by anomalies of the opposite sign over the mid-latitudes of the Atlantic and Asia-Pacific; the anomaly centres seem to shift southwestward over Europe, westward over Asia, and poleward along the Ural mountains and over the Pacific. At sea level, it is associated with decaying anomaly centres moving southeastward over Asia-Pacific, and southwestward over Europe; its high-amplitude phases are characterized by a strong action centre dominating over northern Eurasia, matched by anomalies of opposite sign occurring over the middle-lower latitudes of the European and Pacific sectors. The 35–45 day oscillation is associated with a flow pattern characterized by a blocking structure in the mid-troposphere located over either Europe or Lake Baikal; the related anomaly centres appear to move southwestward over the Pacific, westward over Asia, poleward along the Ural mountains, and southwestward over Europe. At sea level, the anomaly centres associated with this 35–45 day oscillation appear to displace equatorward over Asia, eastward over the Pacific, and southwestward over Europe; the high-amplitude phases are characterized by a strong action centre dominating over northern Eurasia, with weakening anomalies of the opposite sign occurring simultaneously over the subtropics of east Asia-Pacific and Europe. In terms of the wave structures and wave propagation over the Eurasia sector, these two oscillations coincide with previously reported low-frequency oscillations with similar periods at the 700 hPa level. Moreover, the high-amplitude phases of the 35–45 day oscillation are intimately associated with conspicuous anomalies of precipitation over China.

* Corresponding author.

## 1. Introduction

In the last 10 years or more, numerous studies have focused on the description of the spatial structures of atmospheric low-frequency variability by using cross-correlation functions (Wallace and Gutzler, 1981) and empirical orthogonal functions (Barnett and Preisendorfer, 1978; Horel, 1981; Mo and Ghil, 1987; Barnston and Livezey, 1987). Recently, the exploration of low-frequency variability has been addressed in terms of clusters that define recurrent states of the atmosphere and of quasi-stationary weather patterns (Legras et al., 1987; Mo and Ghil, 1988; Molteni et al., 1990; Reinhold and Pierrehumbert, 1982; Vautard and Legras, 1988; Vautard, 1990; Kimoto and Ghil, 1993a and 1993b; Hansen, 1993). Also, using a linear budget technique, Branstator (1992) investigated the maintenance mechanisms of four prominent low-frequency perturbation patterns in a perpetual January general circulation model simulation with fixed ocean temperatures. Most of these studies were based on monthly mean data series, generally with more attention paid to the Northern Hemisphere wintertime. After ascertaining dominant spatial patterns of large-scale anomalies in each of the four seasons, Corte-Real et al. (1995) have also identified modes of non-seasonal atmospheric variability on time scales of the order of a pentad or longer, by means of principal component analysis (PCA). So far, emphasis has been put on the spatial aspects of low-frequency variability and, in spite of noticeable differences among the results, all these studies indicate that the low-frequency extratropical atmosphere likely prefers a small number of states, generally called weather regimes, and a major portion of the variability is contributed by the alternation between these regimes. However, the transitions between the weather regimes are still poorly understood. It is necessary to ascertain the low-frequency time behaviour. In this respect, complex principal component analysis has allowed the detection of some propagative patterns, although with little temporal regularity (Horel, 1984; Branstator, 1987; Lanzante, 1990).

To document the most regular coherent space-time patterns of low-frequency variability, the multi-channel version of Singular Spectrum Analysis (MCSSA) has been developed and applied (Plaut and Vautard, 1994) to a 32-year long set of daily 700-hPa geopotential heights respectively over the Atlantic sector (30° N–70° N, 80° W–40° E), the Pacific sector (30° N–70° N, 140° E–100° W) and the whole extratropical Northern Hemisphere (30° N–80° N). The values used were extracted from the *daily* series with *a low sampling rate of 5 days* and consisting of two shifted $10° \times 10°$ grids; three major low-frequency oscillations (LFOs) were found, with periods of 70 days, 40–45 days, and 30–35 days. Also, it has been reported that: (i) the 70-day oscillation consists of fluctuations in both position and amplitude of the Atlantic jet, with a poleward-propagating anomaly pattern; (ii) the 40–45-day oscillation is specific to the Pacific sector and consists of a monopole pattern drifting westward, with a pronounced Pacific/North American (PNA) structure in its high-amplitude phase; (iii) the 30–35-day mode, consisting of the retrogression of a dipole pattern, is confined over the Atlantic region (likely to be a harmonic of the 70-day mode), the occurrence of the Euro-Atlantic blocking regime being strongly favoured by particular phases of this mode. Nevertheless, there is still little knowledge of the low-frequency time behaviour of the atmosphere over the Eurasia-Pacific sector. The main aim of the current study is to ascertain which low-frequency oscillations dominate over the Eurasia-Pacific sector, how the associated wave motions behave, and hence, to figure out some intermittently regular evolutionary processes of large-scale circulation systems likely to be related to the Asian monsoon variability. For these purposes, multi-channel singular spectrum analysis (MCSSA) is an effective technique and, therefore, was adopted in this study. Nearly periodic components of atmospheric flow behave more regularly in time and, consequently, are more predictable and can be more easily simulated. Therefore, despite the possibility of intermittency, knowledge of low-frequency oscillations over Eurasia-Pacific is useful for improving long-range and even medium-range forecasting of Asian monsoon activity.

## 2. Data base and strategy

The data base for the current study is the NMC daily grid point data of 500-hPa geopotential heights for 43 years (1946–1988), pre-treated by

Corte-Real et al. (1995), and daily grid point data of the sea level pressure field for the same period, provided by NCAR. To reduce the high-frequency transient components and, furthermore, to retain as much information about the low-frequency variability as possible, *5-day-mean* values of grid point data for both 500-hPa geopotential height (Z500) and sea level pressure (SLP) fields, respectively consisting of $5° \times 4°$ and $5° \times 5°$ grids, are chosen for the present study. This is instead of the daily values extracted with a sampling rate of 5 days (daily-values/5-day), on which the pioneer study of Plaut and Vautard (1994) was based (even so, similar computations were also performed on such daily-values/5-day, but with much poorer results). Therefore, the sample size $N$ is 3139-pentad for both the Z500 and SLP fields. The Eurasia-Pacific sector extends from 18° N (Z500) or 20° N (SLP) to 90° N and from 0° E to 180° E.

To compress as much information as possible into a small number of spatial variables, a prior PCA was carried out on the 5-day-mean fields of 500-hPa geopotential height (Z500) and sea level pressure (SLP) respectively, and the eigenvalues were sorted in decreasing order. The resulting first 30 spatial principal components (S-PCs), explaining respectively 98.80% (Z500) and 97.45% (SLP) of the total variances, have been retained as the spatial variables of the relevant fields for the subsequent MCSSA. In other words, the first 30 S-PCs of the Z500 or SLP fields constitute the multi-channel series $X$. Thus, the number of channels, here denoted by $L$, is 30 ($L=30$). Multi-channel singular spectrum analysis (MCSSA) aims first to solve the eigenvalue problem of matrix $T_X$:

$$T_X = \begin{bmatrix} T_{11} & T_{12} & \cdots & T_{1L} \\ T_{21} & T_{22} & \cdots & T_{2L} \\ \vdots & \vdots & \cdots & \vdots \\ T_{L1} & T_{L2} & \cdots & T_{LL} \end{bmatrix},$$

where

$$T_{ll'} = \begin{bmatrix} C^{ll'}_{0,0} & C^{ll'}_{0,1} & \cdots & C^{ll'}_{0,M-2} & C^{ll'}_{0,M-1} \\ C^{ll'}_{1,0} & C^{ll'}_{0,0} & C^{ll'}_{0,1} & \cdots & C^{ll'}_{0,M-2} \\ \vdots & \ddots & \ddots & \ddots & \vdots \\ C^{ll'}_{M-2,0} & \cdots & C^{ll'}_{1,0} & C^{ll'}_{0,0} & C^{ll'}_{0,1} \\ C^{ll'}_{M-1,0} & C^{ll'}_{M-2,0} & \cdots & C^{ll'}_{1,0} & C^{ll'}_{0,0} \end{bmatrix}$$

and

$$C^{ll'}_{j,j'} = \frac{1}{N-|j-j'|} \times \sum_{i=1}^{N-|j-j'|} X_{l,i} X_{l',i+j-j'} \quad (1)$$

$j, j' = 0, 1, \ldots, (M-1)$ (time lags),

$l, l' = 1, 2, \ldots, L$ (channels).

The $X_{l,i}$ in (1) is the value of the $l$th channel variable S-PC$_l$ at time $i$, an element of the matrix $X$; the matrix $T_{ll'} = \{C^{ll'}_{j,j'}\}_{M \times M}$ actually contains the lagged covariances between the $l$th and $l'$th channel variables (i.e., S-PC$_l$ and S-PC$_{l'}$). The $C^{ll'}_{j,j'}$ in (1) have the same value so long as the time lag $|j-j'|$, between the $l$th and $l'$th channel variables, is equal to the same constant; thus, the matrix $T_{ll'}$ is a Toeplitz matrix — a matrix of elements constant along the upper-left to lower-right diagonals. All the Toeplitz matrices $T_{ll'}$ ($l, l' = 1, 2, \ldots, L$; there are $L \times L$ matrices in total) constitute a block-Toeplitz matrix $T_X = \{T_{ll'}\}_{L \times L}$, a matrix with all its elements being a Toeplitz matrix. It represents both the concurrent and lagged correlations between two of the $L$-channel variables (the Toeplitz matrix on the diagonal, $T_{ll}$, contains the lagged autocorrelations of the $l$th channel variable). Solving the eigenvalue problem of the block-Toeplitz matrix $T_X$ results in time sequences of eigenvectors; each time sequence, called a spatial-temporal eigenvector or ST-EOF, is composed of $M$ eigenvectors; each eigenvector in such a time sequence corresponds to a time lag $j$, with $j=0, 1, 2, \ldots, M-1$; $M$ is called window length. Each sequence of eigenvectors, i.e., each ST-EOF, depicts both the changes among grid-points and those from one time step to another, that is, the spatial-temporal variations or wave structure and its propagation in the atmosphere. The relevant principal components are referred to as spatial-temporal principal components (ST-PCs). The associated eigenvalues are sorted in decreasing order and normalized in such a way that they represent fractions of the total variance.

Since singular spectrum analysis will correctly isolate the intermittent oscillation if the window length $M$ is chosen between the period of the oscillation and the average life time of its spells (impossible to know a priori), and is typically successful in analysing periods in the range $(M/5, M)$ (Vautard et al., 1992a), a window length of 80 pentads ($M = 80$-pentad) was first used to isolate and remove the permanent annual cycle and its harmonics. Then, a window length of 35 pentads is chosen as the basic window length of current MCSSA, to isolate the intra- and inter-seasonal oscillations, i.e., oscillations with periods of 35 to 170 days. To confirm the plausibility of the oscillations obtained, MCSSA experiments with a window length of 28-pentad were also carried out.

In order to remove the annual cycle and its harmonics, the following reconstruction technique developed by Plaut and Vautard (1994) was first used to obtain the $k$th reconstructed component $\mathrm{RC}_k = \{R^k_{li}\}$ at time $i$ for channel $l$:

$$R^k_{li} = \frac{1}{i}\sum_{j=1}^{i} a^k_{i-j} E^k_{lj},$$

$$\text{when} \quad 1 \leqslant i \leqslant M-1, \tag{2a}$$

$$R^k_{li} = \frac{1}{M}\sum_{j=1}^{M} a^k_{i-j} E^k_{lj},$$

$$\text{when} \quad M \leqslant i \leqslant N-M+1, \tag{2b}$$

$$R^k_{li} = \frac{1}{N-i+1}\sum_{j=i-N+M}^{M} a^k_{i-j} E^k_{lj},$$

$$\text{when} \quad N-M+2 \leqslant i \leqslant N, \tag{2c}$$

where $a^k_{i-j}$ denotes the $k$th ST-PC (or ST-PC$_k$), and $E^k_{lj}$ the associated $k$th ST-EOF (or ST-EOF$_k$); then, the original multi-channel series $\boldsymbol{X}$ (i.e., the first 30 S-PCs of the Z500 or SLP fields) were split into

$$\boldsymbol{X} = \boldsymbol{Y} + \boldsymbol{Z} \tag{3}$$

where

$$\boldsymbol{Y} = \{Y_{li}\}, \qquad Y_{li} = \sum_n R^n_{li} \tag{3a}$$

$$\boldsymbol{Z} = \boldsymbol{X} - \boldsymbol{Y}. \tag{3b}$$

In eqs. (3), $n$ denotes a family of the reconstructed components $\mathrm{RC}_k = \{R^k_{li}\}$ $(k = 1, 2, ..., n)$, comprising those RCs which correspond to the annual cycle and its harmonics. So, $\boldsymbol{Z}$ is the adaptively filtered series that will be used for improving the localisation of oscillations with periods in the range 28–170 days, the adaptive filter being directly provided by the antecedent MCSSA. For the Z500 fields, the $n$ family consists of the RCs of orders 1–4 (annual cycle and its second harmonic), and for the SLP fields, it comprises the RCs of orders 1–2 (annual cycle). Considering the possible phase shift near the ends of the reconstructed series RCs (cf. eqs. (2a) and (2c)), in which the number of eigenelements used is less than $M = 80$), the 80 data values at the two ends of the $L$-channel series $\boldsymbol{Z}$ were not used in the subsequent MCSSA experiments (with $M = 35$ or 28 pentads). Also, MCSSA experiments were carried out on a filtered series in which the annual cycle represented by a Fourier expansion in the time domain is removed (a different algorithm for removing the annual cycle).

The fundamental property of MCSSA lies in the fact that when (i) two consecutive eigenvalues are nearly equal, (ii) the two corresponding time sequences of eigenvectors (the corresponding ST-EOF pair) are nearly periodic, with the same period, and in quadrature, displaying the same spatial-temporal patterns, (iii) the associated pair of ST-PCs are in quadrature, then there is in the multi-channel series an oscillation whose period is the same as the period of the ST-EOF pair themselves, and whose spatial-temporal patterns are the same as those represented by any sequence of the ST-EOF pair (Plaut and Vautard, 1994). Therefore, a pair of eigenelements $(k, k+1)$ is selected as an oscillatory pair when: (1) the frequencies $f_k$ and $f_{k+1}$, respectively, corresponding to the maximum spectral values of $\mathrm{ST}-\mathrm{PC}_k$ and ST-PC$_{k+1}$ satisfy $2M\,|f_k - f_{k+1}| < 0.75$ (Vautard et al., 1992a); (2) the two successive extrema, on each side of 0, of the lagged correlation between $\mathrm{ST}-\mathrm{PC}_k$ and $\mathrm{ST}-\mathrm{PC}_{k+1}$ are larger than 0.5 in absolute value, i.e., the lagged correlation itself has an oscillatory behaviour, with at least one cycle being coherent; (3) there is at least one complete cycle, of period $T = 1/f^*$ ($f^*$ is the peak frequency between $f_k$ and $f_{k+1}$), clearly existing in the pair of eigenvector time-sequences, $\mathrm{ST}-\mathrm{EOF}_k$ and $\mathrm{ST}-\mathrm{EOF}_{k+1}$.

Maximum entropy (ME) spectrum analysis based on the formulation of Barrodale and Erickson (1980) was used in combination with MCSSA, to estimate power spectra; the period of the oscillation corresponding to the pair of order $(k, k+1)$ is estimated as the peak location of the sum, $P^k(f) + P^{k+1}(f)$, of the ME power spectra of $\mathrm{ST}-\mathrm{PC}_k$ and $\mathrm{ST}-\mathrm{PC}_{k+1}$. The fraction $r_{k,k+1}(f)$ of the variance explained by the oscillation, at frequency $f$, is equal to the sum $P^k(f)+P^{k+1}(f)$ divided by the total spectrum $M \times P(f)$:

$$M \times P(f)=\sum_{k=1}^{L \times M} P^k(f), \tag{4a}$$

$$r_{k,k+1}(f)=\frac{[P^k(f)+P^{k+1}(f)]}{[M \times P(f)]}. \tag{4b}$$

To check whether the periodicities detected are reproducible, both the Z500 and SLP series for 1946–1988 (hereafter called the basic dataset) were split into two equal parts, i.e., from 1947 to 1967 and from 1968 to 1988 (hereafter referred to as dataset-1 and dataset-2); then, PCA and MCSSA were performed on each part separately. Moreover, to examine the robustness of the isolated oscillations, similar MCSSA experiments were carried out on a *randomly resampled* basic dataset (1946–1988), and on a dataset *scrambled* as follows: the order of the time series of the channels 2, 4, 6, ..., 30 is reversed, so that the dataset is scrambled; in this process, the correlation between some channels is destroyed, but the autocorrelation property of each channel is retained.

Furthermore, to obtain reliable information about the amplitude of the low-frequency oscillation, composites of the raw Z500 or SLP anomalies (i.e., deviations from the climatological mean of relevant pentad) keyed to eight equally populated phase-categories of the oscillations were carried out *season by season*, with the phase-categories being defined by using the reconstructed components (RCs), which are directly comparable with the multi-channel series (i.e., S-PCs). More precisely, the instantaneous phase $\phi_i$ of the oscillation at time $i$ is defined as

$$\tan \phi_i=\frac{Y_{li}}{Y'_{li}}, \tag{6}$$

where $l$ is the channel for which the variance of $Y_l=\{Y_{li}=R^k_{li}+R^{k+1}_{li};\, i=1, 2, ..., N\}$ is maximal, and $Y'_l=\{Y'_{li}\}$ is the time derivative of $Y_l$, estimated by centred finite differences; the interval $(0, 2\pi)$ is split into eight intervals in such a way that the same number of values of $\phi_i$ falls within each interval. Thus, the atmosphere spends approximately an equal time in each phase of the eight categories. More detailed description of MCSSA can be found in the pioneer paper by Plaut and Vautard (1994).

## 3. Low-frequency oscillations over Eurasia

### *3.1. Annual cycle and its harmonics*

All oscillatory pairs identified by MCSSA with a window length of 80 pentads, from the basic dataset (1946–1988) as well as from dataset-1 (1947–1967) and dataset-2 (1968–1988), together with the relevant peak variance fractions, are listed in Table 1. As can be seen from this table, both in the mid-troposphere and at sea level, the annual cycle (365 days) is reproducible, while a 181-day oscillation is present only in the mid-troposphere;

Table 1. *Oscillatory pairs, identified from the MCSSA experiments with $M=80$-pentad, and their peak variance fractions (in parentheses)*

| | Basic dataset | | Dataset-1 | | Dataset-2 | |
|---|---|---|---|---|---|---|
| | pair | periods in day | pair | periods in day | pair | periods in day |
| Z500 | 1–2 | **365** (99.98%) | 1–2 | **365** (99.99%) | 1–2 | **365** (99.99%) |
| | 3–4 | **181** (94.75%) | 3–4 | **181** (95.06%) | 3–4 | **181** (94.11%) |
| | 20–21 | 158 (28.79%) | 18–19 | 145 (38.59%) | 15–16 | 88 (57.26%) |
| | 9–10 | 110 (68.64%) | 6–7 | 122 (81.08%) | | |
| SLP | 1–2 | **365** (99.94%) | 1–2 | **365** (99.97%) | 1–2 | **365** (99.92%) |
| | 4–5 | 202 (45.06%) | 6–7 | 242 (21.66%) | 3–4 | 195 (91.02%) |
| | 13–14 | 145 (60.34%) | 9–10 | 151 (64.01%) | 19–20 | 125 (40.42%) |
| | 6–7 | 94 (86.06%) | 4–5 | 100 (43.87%) | 9–10 | 91 (56.84%) |

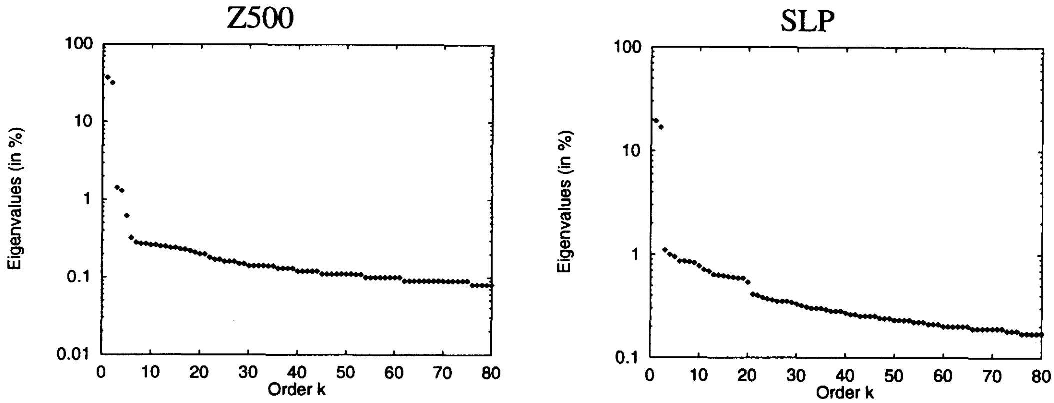


*Fig. 1.* Eigenvalue spectra of the basic Z500 and SLP datasets, derived by MCSSA with a window length of 80 pentads.

no other inter-seasonal oscillations (with periods longer than 80 days) are reproducible. Therefore, only the annual cycle at both levels and the mid-tropospheric 181-day oscillation will be regarded as robust and discussed further. Fig. 1 shows the eigenvalue spectra of the Z500 and SLP field-series for 1946–1988.

As listed in Table 1, the permanent annual cycle at both levels, together with their inter-annual variabilities, was well isolated as the most robust oscillatory pair, pair 1–2, whose eigenvalues clearly stand out of the spectra (Fig. 1). In the mid-troposphere, this cycle is associated with a global increase of the isosurface's height during warming seasons alternating with a global decrease in wintertime, as well as westerly planetary wave activities over Eurasia, exhibiting the transition processes between the wintertime eastern Asian trough, matched by the western European ridge, and the summer-time eastern Asian ridge accompanied by the western European trough. As represented by the corresponding eigenvector-sequence ST-EOF01 or ST-EOF02 (not shown), fully developed quasi-stationary westerly troughs (ridges) will normally be replaced by mature ridges (troughs) in 6 months. At sea level, the transition process is reflected in the seasonal alternations of the quasi-stationary action centres over the Eurasia sector, such as the Asian continental heat low or cold high and the Aleutian and Icelandic lows. As represented in the relevant eigenvector-sequence ST-EOF01 or ST-EOF02 (not shown), the Asian continental heat low occurs simultaneously with a weakened Aleutian low, which alternates in 6 months with the Asian continental cold high matched by a deepened Aleutian low.

In the mid-troposphere, the 2nd robust oscillatory pair (pair 3–4) represents a 181-day oscillation, contributing 94.75 % to the variance in the relevant frequency band. Checking for phase locking between pair 1–2 and pair 3–4 in the mid-troposphere (Fig. 2), one can clearly see that this oscillatory pair (pair 3–4) actually represents the second harmonic of the annual cycle (pair 1–2). Since symmetric phases of this oscillation exhibit structures of opposite phases, it is sufficient to show half a complete cycle. Four phases in half a complete cycle of this oscillation (with an

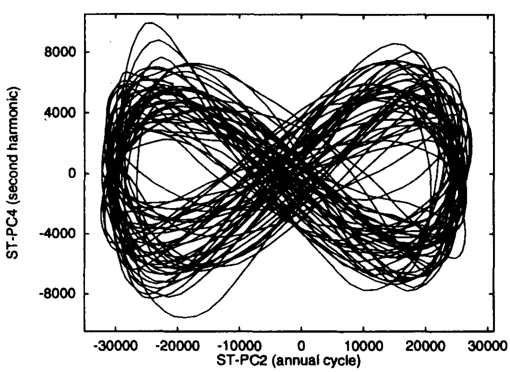


*Fig. 2.* Time evolution of ST-PC4 versus ST-PC2 derived from performing MCSSA on the Z500 field-series (43 years), with a window length of 80 pentads.

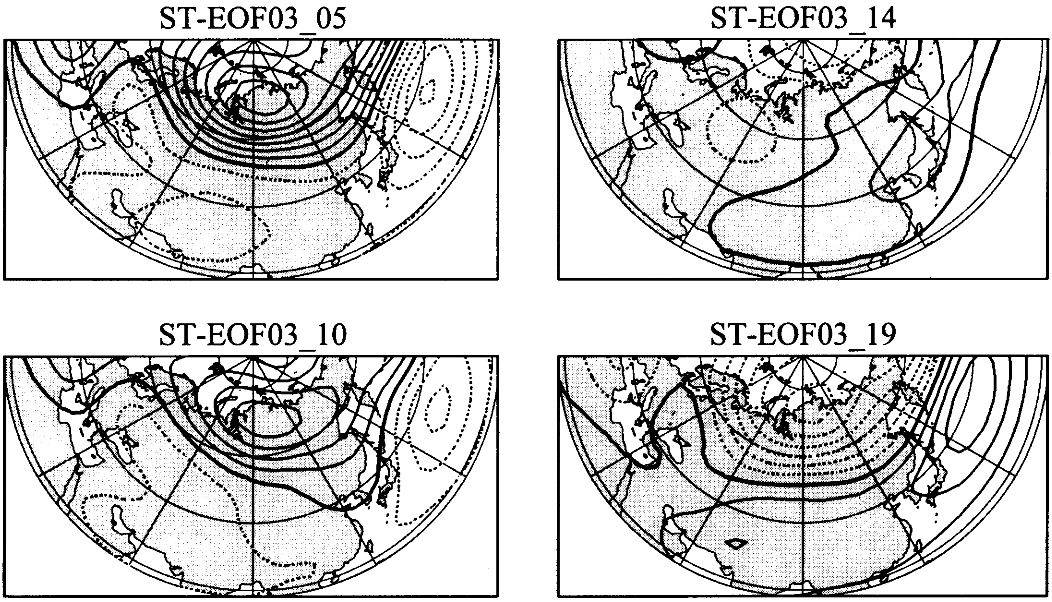


*Fig. 3.* Spatial-temporal structures of the 180–185 day oscillation in the mid-troposphere, represented by the eigen-vector-sequence ST-EOF03 derived from MCSSA performed on the Z500 field-series, with a window length of 80 pentads.

interval of 4 or 5 pentads between maps) are shown in Fig. 3, from which one can see that while the Pacific subtropical high strengthens and the Eurasian jet intensifies, receding northward, the Siberian high decays and the polar vortex deepens; conversely, when the Siberian high strengthens and the Pacific subtropical high weakens, the Eurasian jet reduces and shifts southward. At sea level, no semi-annual fluctuation was identified.

### 3.2. *Intra-seasonal oscillations over Eurasia*

As explained in Section 2, for an accurate localisation of low-frequency oscillations with periods in the range 28–170 days, the reconstructed components (RCs) of orders $1 \sim 4$ (Z500) or $1 \sim 2$ (SLP) of the antecedent experiments of MCSSA, i.e., the annual cycle and its second harmonic, were removed from the relevant datasets, and MCSSA experiments with window lengths of 35 and 28 pentads were then carried out on the filtered datasets (i.e., basic dataset, dataset-1 and dataset-2) respectively. Oscillatory pairs satisfying criteria given in Section 2, together with their peak variance fractions, are listed in Table 2; the ST-PCs corresponding to similar periods obtained from both the basic dataset (Z500 or SLP) and its subsets, or from MCSSA experiments with two different window lengths (e.g., mid-tropospheric pair 2–3 of basic dataset, pair 4–5 of dataset-1, and pair 1–2 of dataset-2; surface pair 5–6 of both basic dataset and dataset-1, and pair 4–5 of dataset-2; etc.) are significantly correlated to each other (at a confidence level of 99%), indicating that they represent the same oscillation. Thus it is clear that two low-frequency oscillations (with periods of 55–65 and 35–45 days) are reproducible at both levels, when different window lengths are used and when MCSSA is applied to the two subsets of the filtered basic data series, namely filtered dataset-1 and dataset-2 (see Table 2). Furthermore, a 100–110 day oscillation seems to be reproducible in the mid-troposphere.

However, when the filtered basic datasets are scrambled (cf. Section 2), the periods obtained from the scrambled datasets (listed in Table 3) are *irreproducible* when using different window lengths (35 and 28 pentads). Furthermore, when the filtered basic datasets are *randomly resampled*, the resulting reproducible period is 30–32 days for both the resampled Z500 and SLP field-series (see also Table 3), which is qualitatively different from the reproducible quasi-periodicities (55–65 and

Table 2. *Oscillatory pairs and their peak variance fractions (in parentheses), identified from the MCSSA experiments with different window lengths, performed on the 6 filtered datasets (basic dataset, dataset-1 and dataset-2 for the both levels)*

| Z500 | | | | SLP | | | |
|---|---|---|---|---|---|---|---|
| $M = 35$ pentads | | $M = 28$ pentads | | $M = 35$ pentads | | $M = 28$ pentads | |
| pair | periods in day | pair | periods in day | pair | periods in day | pair | periods in day |
| Filtered basic dataset (1946–1988) | | | | | | | |
| 21–22 | 116 (13%) | | | 9–10 | 180 (36%) | 3–4 | 95 (63%) |
| 4–5 | **101** (69%) | | | 3–4 | 91 (76%) | 13–14 | 81 (38%) |
| 2–3 | **58** (53%) | 2–3 | **59** (71%) | 5–6 | **60** (42%) | 5–6 | **61** (31%) |
| 10–11 | **37** (55%) | 8–9 | **41** (36%) | 11–12 | **37** (31%) | 10–11 | **35** (20%) |
| | | | | | | 19–20 | 44 (26%) |
| Filtered dataset-1 (1947–1967) | | | | | | | |
| 2–3 | **97** (65%) | 2–3 | **110** (63%) | 2–3 | 96 (77%) | | |
| 4–5 | **63** (49%) | 4–5 | **62** (29%) | 5–6 | **65** (30%) | 4–5 | **63** (18%) |
| 11–12 | **37** (33%) | 8–9 | **37** (56%) | 16–17 | **40** (22%) | 13–14 | **41** (29%) |
| Filtered dataset-2 (1968–1988) | | | | | | | |
| 6–7 | **100** (60%) | 5–6 | **110** (50%) | | | 12–13 | 79 (16%) |
| 1–2 | **58** (75%) | 1–2 | **59** (67%) | 4–5 | **61** (80%) | 3–4 | **61** (87%) |
| 9–10 | **38** (49%) | 7–8 | **41** (37%) | 11–12 | **35** (61%) | 10–11 | **35** (43%) |

Table 3. *Reproducible quasi-periodicities of the filtered basic datasets, and oscillatory pairs obtained from the scrambled or randomly resampled basic datasets (with their peak variance fractions given in the parentheses)*

| Z500 | | | | SLP | | | |
|---|---|---|---|---|---|---|---|
| $M = 35$ pentads | | $M = 28$ pentads | | $M = 35$ pentads | | $M = 28$ pentads | |
| pair | periods in day | pair | periods in day | pair | periods in day | pair | periods in day |
| Filtered basic dataset (1946–1988) | | | | | | | |
| 4–5 | **101** (69%) | | | | | | |
| 2–3 | **58** (52%) | 2–3 | **59** (71%) | 5–6 | **60** (42%) | 5–6 | **61** (31%) |
| 10–11 | **37** (55%) | 8–9 | **41** (36%) | 11–12 | **37** (31%) | 10–11 | **35** (20%) |
| Scrambled basic dataset (1946–1988) | | | | | | | |
| 3–4 | 60 (43%) | 12–13 | 36 (38%) | 8–9 | 184 (46%) | 3–4 | 96 (65%) |
| | | | | | | 17–18 | 52 (39%) |
| | | | | | | 9–10 | 43 (15%) |
| Randomly resampled basic dataset (1946–1988) | | | | | | | |
| 13–14 | 30 (5%) | 9–10 | 32 (10%) | 36–37 | 31 (17%) | 29–30 | 32 (31%) |
| | | | | | | 2–3 | 38 (18%) |

Table 4. *Oscillatory pairs and their peak variance fractions (in parentheses), obtained from the MCSSA experiments performed on the filtered basic series in which the annual cycle removed was represented by a Fourier expansion in the time domain*

| Z500 (1946–1988) | | | | SLP (1946–1988) | | | |
|---|---|---|---|---|---|---|---|
| $M = 35$ pentads | | $M = 28$ pentads | | $M = 35$ pentads | | $M = 28$ pentads | |
| pair | periods in day | pair | periods in day | pair | periods in day | pair | periods in day |
| 7–8 | **62** (60%) | 6–7 | **62** (56%) | 7–8 | **61** (47%) | 7–8 | **61** (26%) |
| 14–15 | **38** (44%) | 12–13 | **39** (39%) | 13–14 | **42** (23%) | 19–20 | **42** (22%) |

35–45 days) of the filtered basic datasets. Also, when the MCSSA experiments are performed on a filtered basic field-series in which the annual cycle represented by a Fourier expansion in the time domain is removed, the quasi-periodicities of 55–65 and 35–45 days are also identified at both levels, but the 100–110 day period is not found (see Table 4). It can therefore be concluded that, both in the mid-troposphere and at sea level, there exist two robust oscillations over the Eurasian sector, with quasi-periods of 55–65 and 35–45 days. These two intermittent oscillations can be well represented by the oscillatory pairs derived from MCSSA experiments with $M = 35$ pentads, that is, pairs 2–3 and 10–11 in the mid-troposphere, and pairs 5–6 and 11–12 at sea level; the relevant variance fractions in the frequency domain are shown in Fig. 4 (the percentages of variance refer to the total variance of adaptively filtered datasets). Moreover, the mid-tropospheric 58-day and surface 60-day oscillations, or the 37-day oscillation at both levels, are actually the same oscillation, since the relevant ST-PCs are significantly correlated to each other (see Table 5). No phase locking between the relevant oscillatory pairs of these two quasi-periodicities was found, indicating that the 35–45 day oscillation is not a harmonic of the 55–65 day oscillation.

*3.2.1. The 55–65 day oscillation.* The oscillatory pair 2–3 in the mid-troposphere corresponds to a 55–65 day oscillation, accounting for 53% of the total variance at the relevant peak frequency. This oscillation is associated with transitions between flow regimes of intense anomalies over the polar cap-Ural mountains, matched by anomalies of the opposite sign over the mid-latitudes of the Atlantic and Asia-Pacific; the anomaly centres appear to shift southwestward over Europe, westward over Asia, and poleward along the Ural mountains and

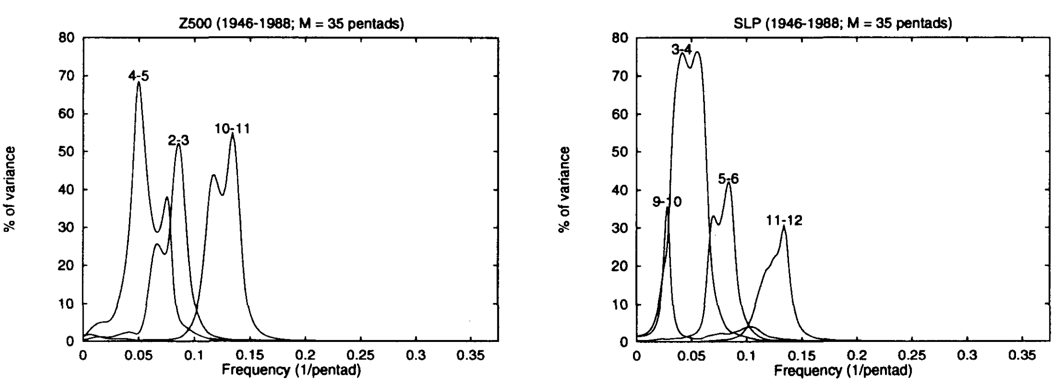


*Fig. 4.* Variance fraction (%) of the indicated pair of ST-PCs of the filtered basic datasets, derived by MCSSA with a window length of 35 pentads.

Table 5. *Concurrent correlation coefficients between mid-tropospheric and surface ST-PCs corresponding to similar periods*

| Z500\SLP | ST-PC5 | ST-PC6 | Z500\SLP | ST-PC11 | ST-PC12 |
|---|---|---|---|---|---|
| ST-PC2 | 0.0555 | 0.7848 | ST-PC10 | −0.6952 | 0.1290 |
| ST-PC3 | −0.6322 | −0.0322 | ST-PC11 | 0.1133 | 0.7312 |

The sample size is $N = 2945$, so that the critical value is about 0.0606 for the 99.9% confidence level.

over the Pacific. Fig. 5 shows 6 phases in half a complete cycle represented by the associated ST-EOF3. Symmetric phases of this oscillation display anomaly patterns of opposite sign. The relevant season-composites indicate that this oscillation behaves more regularly in winter; it is weakest during summer. The amplitude of the composite is maximal in winter, with a positive anomaly of about 90 m over the Kara Sea (78°N, 95°E), occurring simultaneously with negative

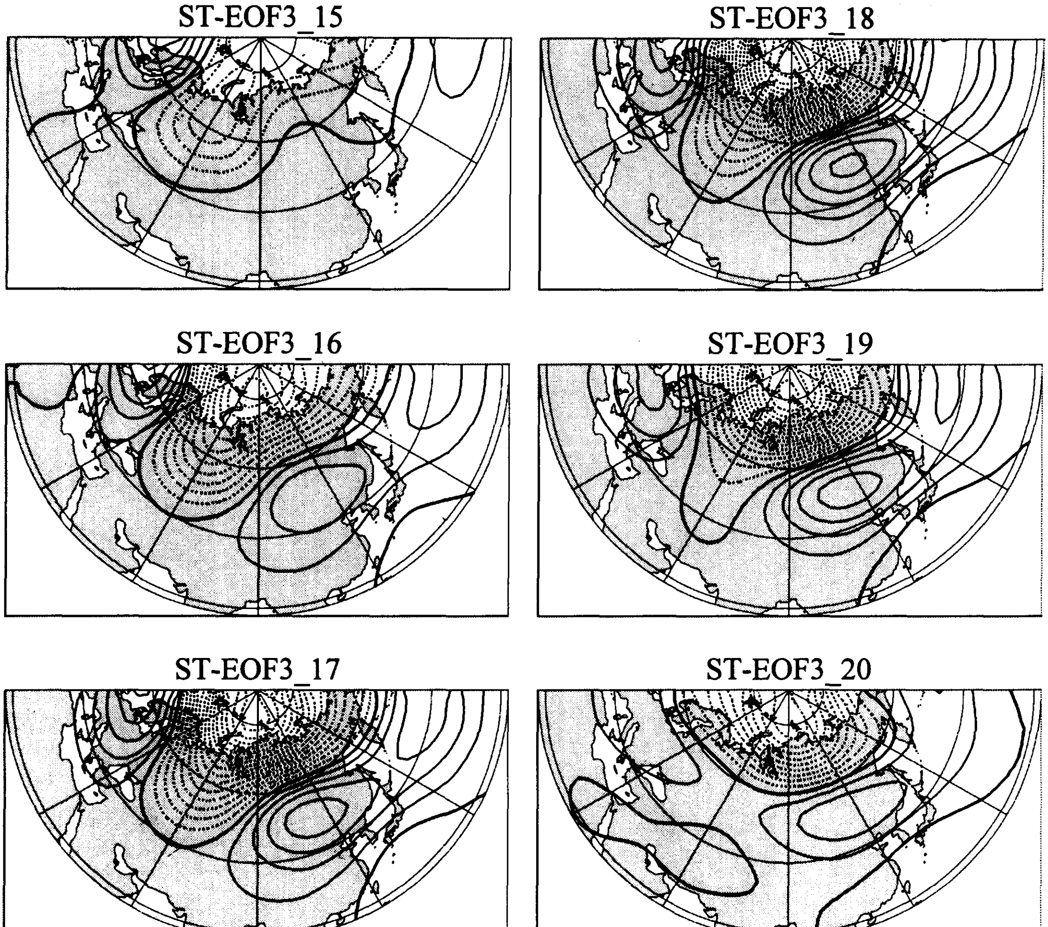


*Fig. 5.* Spatial-temporal structures of the 55–65 day oscillation in the mid-troposphere, represented by the eigen-vector-sequence ST-EOF3 derived from MCSSA performed on the relevant basic dataset Z500, with a window length of 35 pentads.

anomalies of roughly 35 m over the Atlantic and Lake Baikal-central Pacific. The maximum negative anomaly of the composite is $-90$ m, occurring north of Siberia (78° N, 105° E) also in winter, accompanied by a positive anomaly of about 25 m over Lake Baikal. Moreover, in terms of the wave structure and its propagation over the Eurasia sector, this Eurasia 55–65 day oscillation is consistent with the Atlantic 70 day oscillation at the 700 hPa level reported by Plaut and Vautard (1994).

Correspondingly, the 55–65 day oscillation can be represented by pair 5–6 at sea level, with a peak variance fraction of about 42%. The high-amplitude phases of this oscillation are characterized by a strong action centre dominating over northern Eurasia, matched by anomalies of the opposite sign over the middle-lower latitudes of Europe and the Pacific sectors. This oscillation is associated with weakening anomaly centres moving southeastward over the Asia-Pacific sector, and southwestward over Europe. Six phases in half a complete cycle of this oscillation represented by ST-EOF6 are shown in Fig. 6. In particular, when a fully developed anomaly centre over Siberia weakens and displaces southeastward to Asia-Pacific, with a small cell moving southwestward to the Atlantic, anomalies of the opposite sign emerge over the polar cap region, extending to Siberia; as this strengthening action centre develops fully, the 55–65 day oscillation

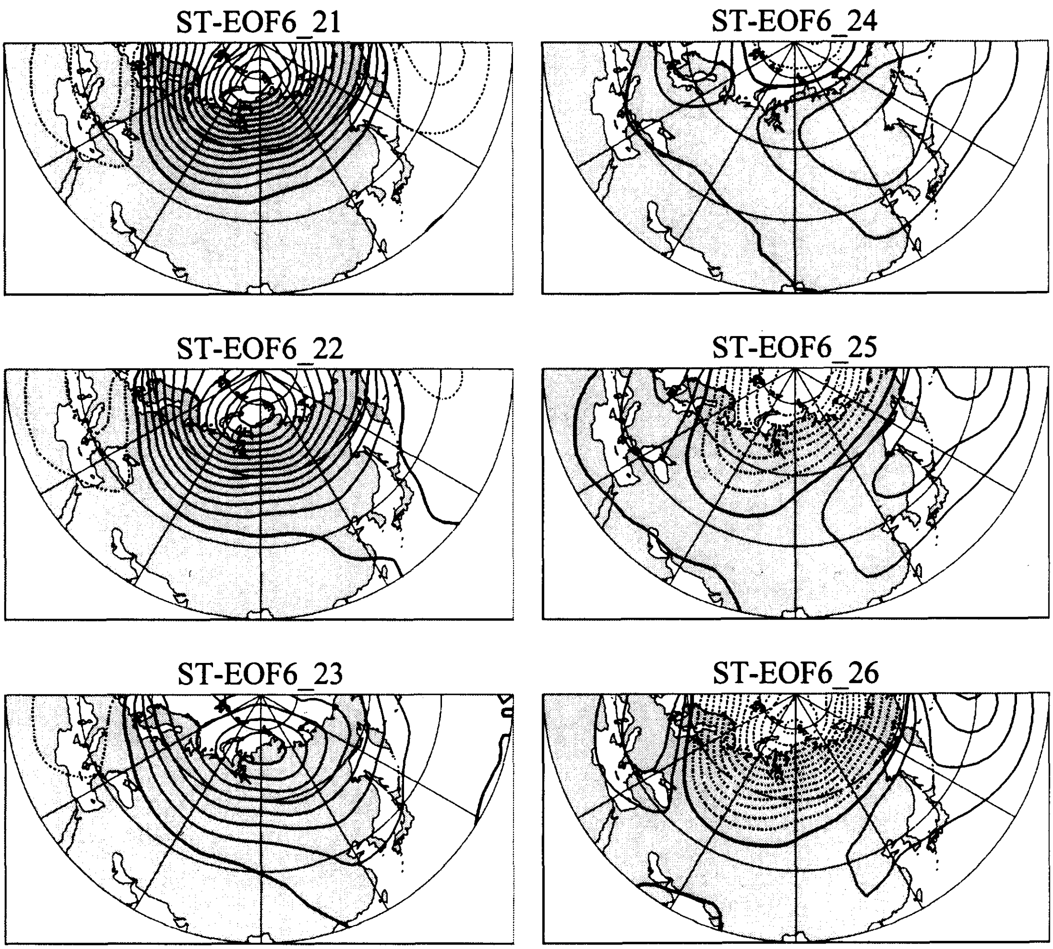


*Fig. 6.* Spatial-temporal structures of the 55–65 day oscillation at sea level, represented by the eigenvector-sequence ST-EOF6 derived from MCSSA performed on the relevant basic dataset SLP, with a window length of 35 pentads.

achieves half a complete cycle. Symmetric phases of this oscillation at sea level also exhibit structures of opposite sign. In autumn, the maximal composite anomaly, +4.48 hPa, occurs over the Aleutian islands (55° N, 170° E); and the maximum negative anomaly is −4.03 hPa, appearing over east of Greenland (80° N, 5° E) in winter.

*3.2.2. The 35–45 day oscillation.* The 35–45 day oscillation was isolated respectively as pair 10–11 in the mid-troposphere and as pair 11–12 at sea level, explaining about 55% (Z500) and 31% (SLP) of the variances at the relevant peak frequency.

In the mid-troposphere, as shown in Fig. 7, the 35–45 day oscillation is associated with a flow pattern of either the European or Lake Baikal blocking structure: the most remarkable action centre dominates over northern Europe (centred over the Barent Sea or Scandinavia), with an action centre of the opposite sign occurring simultaneously over the Altai mountains, Lake Baikal, and eastern Asia (Korea-Japan and eastern China) being in phase with northern Europe. The related anomaly centres appear to move southwestward over the Pacific, westward over Asia, poleward along the Ural mountains, and southwestward over Europe. Symmetric phases of this 35–45 day oscillation also display anomaly patterns of opposite sign. The corresponding season-composites show that this oscillation is most robust in spring and winter, with the maximal composite anomalies dominating over the Barent Sea: −65 m occurs at (78° N, 55° E) in spring, and +57 m appears at (70° N, 35° E) in winter. Besides, in terms of the anomaly pattern and wave propagation over the Eurasia sector, this Eurasia 35–45 day oscillation coincides with the Pacific or global 40–45 day oscillation at the 700 hPa level reported by Plaut and Vautard (1994).

At sea level, the high-amplitude phases of the 35–45 day oscillation are characterized by a strong action centre dominating over northern Eurasia (centred over the Kara Sea), with weakening anomalies of the opposite sign occurring simultaneously over the subtropics of east Asia-Pacific and Europe. The associated anomaly centres appear to displace equatorward over Asia, eastward over the Pacific, and southwestward over Europe. As represented by ST-EOF11 shown in

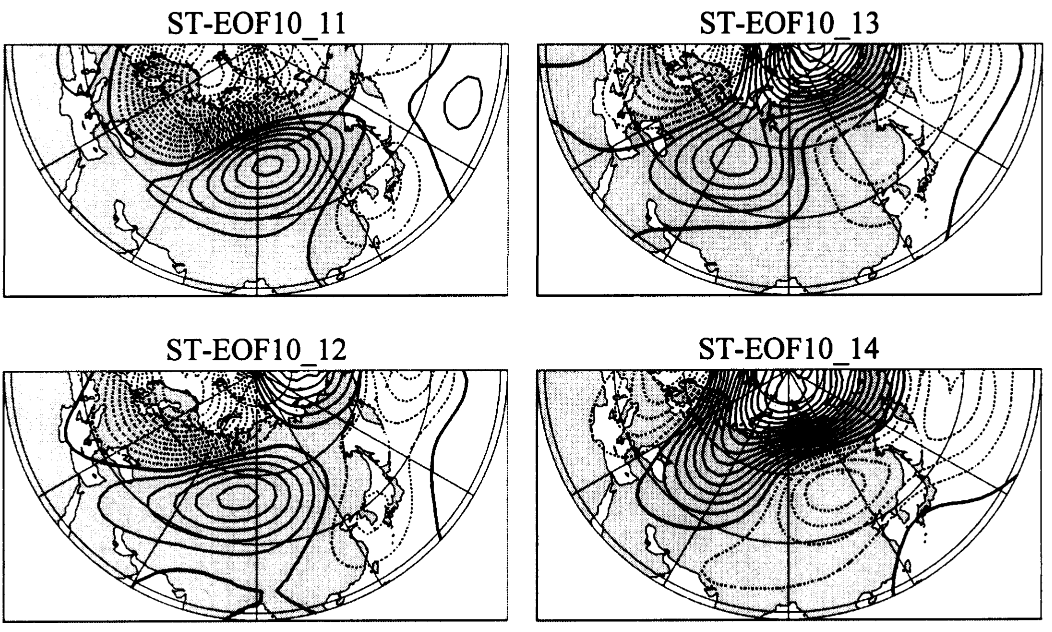


*Fig. 7.* Spatial-temporal structures of the 35–45 day oscillation in the mid-troposphere, represented by the eigenvector-sequence ST-EOF10 derived from MCSSA performed on the relevant basic dataset Z500, with a window length of 35 pentads.

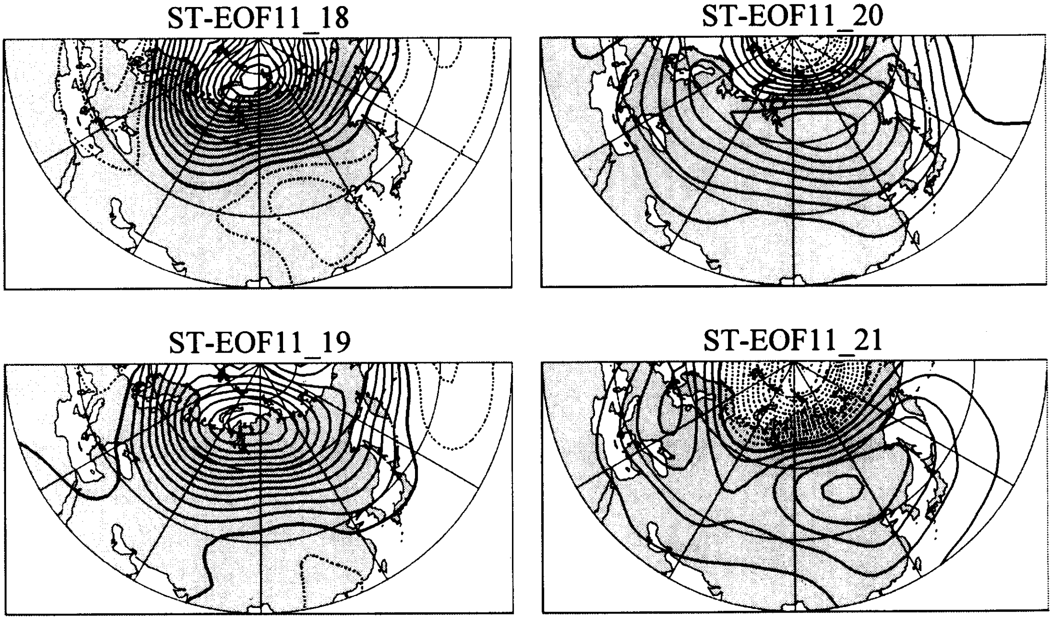


*Fig. 8.* Spatial-temporal structures of the 35–45 day oscillation at sea level, represented by the eigenvector-sequence ST-EOF11 derived from MCSSA performed on the relevant basic dataset SLP, with a window length of 35 pentads.

Fig. 8, when the strong centre of action over the Kara Sea weakens and displaces equatorward to southeastern Asia, anomalies of the opposite sign emerge over the polar cap and fully develop over the Kara Sea, so that the 35–45 day oscillation achieves half a round cycle. Symmetric phases of this oscillation display anomaly structures of opposite sign. The maximal anomaly of the season-composites, −5.85 hPa, appears over north of Siberia (80° N, 120° E) in summer, while +4.47 hPa is the maximum positive anomaly, occurring over Siberia (60° N, 105° E) in winter.

As indicated by the composite maps shown in Fig. 9, the high-amplitude phases of this 35–45 day oscillation in the mid-troposphere display circulation patterns characterized by a blocking high (or deep trough) over northern Europe, occurring simultaneously with a pair of sign-reversed action centres over Asia, i.e., a trough (or ridge) over the Altai mountains or Lake Baikal matched by a ridge (or trough) over eastern Asia; at sea level, these are associated with flow patterns characterized by a north–south dipole over Eurasia: a strong anticyclone (or cyclone) centred over

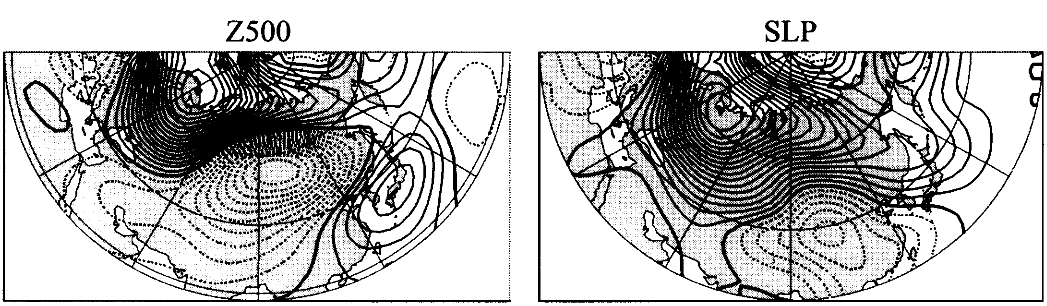


*Fig. 9.* Winter composites of the raw Z500 and SLP anomalies keyed to phase-category 8 of the mid-tropospheric 35–45 day oscillation. Contour intervals: 3.00 m for Z500, 0.30 hPa for SLP. Positive anomalies are represented by continuous contours, and negative anomalies by dashed contours. Bold lines indicate zero anomalies.

(a) modes of concurrent CCA pair 1 between SLP and R5

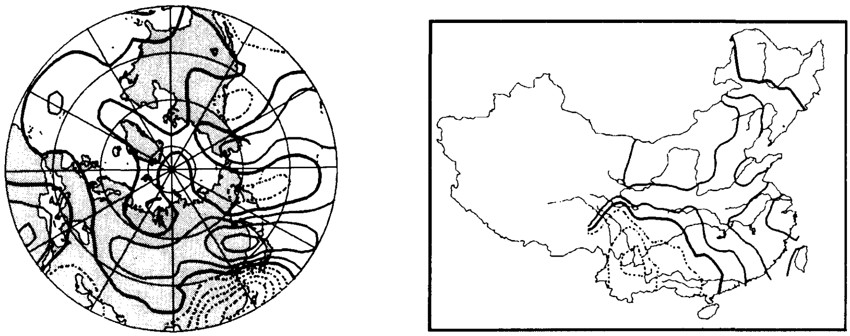

(b) modes of concurrent CCA pair 1 between Z500 and R5

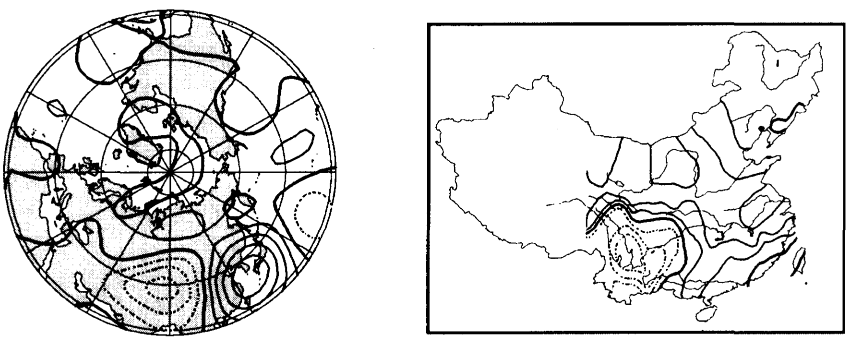

(c) composites of concurrent CCA pair 1 between Z500 and R5 in April-June

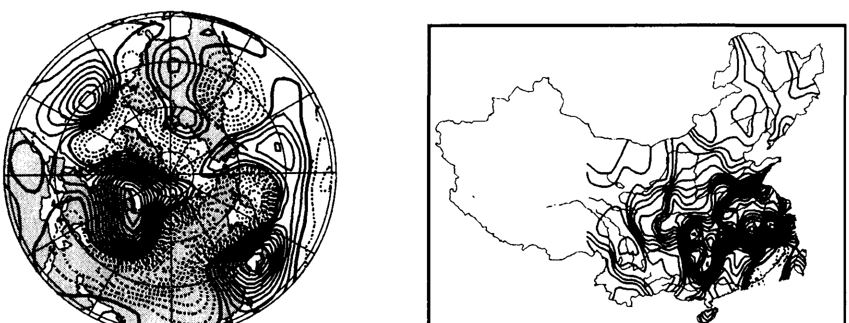

*Fig. 10.* Modes of the concurrent Canonical Correlation (CCA) pair 1 between Z500 or SLP and the 5-day rainfall (R5) over China as well as the associated composite maps of the raw Z500 and R5 deviations (from the climatological annual cycle), keyed to pentads in which the maximal 30 values of the rainfall time series of the CCA modes identified from the season indicated occur. Solid lines indicate positive values, and dashed lines negative values. The zero lines are in bold. The contour intervals of CCA modes are 0.05 for R5 and 0.03 for Z500 and SLP; for the composite maps, the intervals are 2.0 mm (for R5) and 5.0 m (for Z500) respectively (quoted from Wang et al., 1994. Here, modes of a concurrent CCA pair exhibit a concurrent circulation mode responsible for (i.e., intimately correlated with) the relevant rainfall pattern.).

northern Europe occurring simultaneously with a depression (or high pressure) centred over China. Interestingly, such circulation structures, according to Wang et al. (1994), will lead to conspicuous anomalies of precipitation over China: a mid-tropospheric pattern of a trough over the Altai mountains accompanied by a ridge over eastern Asia, matched by positive SLP anomalies over the mid-latitudes of Asia occurring simultaneously with negative SLP anomalies over southern Asia, is associated with more precipitation over the Yangtze-Huaihe and Yellow River basins and less precipitation over southwestern China (see Fig. 10), and vice versa (Wang, et al., 1994); such a circulation pattern is very similar to the "vortices with shear-lines mode", one of the well known characteristic large scale patterns of circulation responsible for most rainstorms over China (Tao et al., 1980).

## 4. Summary

Using multi-channel singular spectrum analysis, the low-frequency variability of circulation over the Eurasian sector has been explored both in the mid-troposphere and at sea level. Two low-frequency oscillations existing at both levels were identified to be robust.

(1) The 55–65 day oscillation: in the mid-troposphere, this is associated with transitions between flow regimes of intense anomalies over the polar cap-Ural mountains, matched by anomalies of the opposite sign over the mid-latitudes of the Atlantic and Asia-Pacific; the anomaly centres seem to shift southwestward over Europe, westward over Asia, poleward along the Ural mountains and over the Pacific. At sea level, it is associated with weakening anomaly centres moving southeastward over Asia-Pacific, and southwestward over Europe; its high-amplitude phases are characterized by a strong action centre dominating over northern Eurasia, matched by anomalies of opposite sign occurring over the middle-lower latitudes of Europe and the Pacific sectors.

(2) The 35–45 day oscillation: this is associated with a mid-tropospheric pattern of either the European or the Lake Baikal blocking structure. The related anomaly centres appear to move southwestward over the Pacific, westward over Asia, poleward along the Ural mountains, and southwestward over Europe. At sea level, the associated anomaly centres appear to displace equatorward over Asia, eastward over the Pacific, and southwestward over Europe; the high-amplitude phases are characterized by a strong action centre dominating over northern Eurasia, with weakening anomalies of the opposite sign occurring simultaneously over the subtropics of east Asia-Pacific and Europe.

These two low-frequency oscillations are not only reproducible, but also qualitatively different from those obtained from scrambled or randomly resampled datasets. They are more robust and behave more regularly in winter and/or in spring. In terms of the wave structures and wave propagation over the Eurasia sector, the 55–65 day oscillation is in concert with the Atlantic 70 day oscillation at the 700 hPa level reported by Plaut and Vautard (1994), and the 35–45 day oscillation coincides with their 40–45 day oscillation over the Pacific sector and over the northern hemisphere. Moreover, the high-amplitude phases of the 35–45 day oscillation are intimately associated with conspicuous anomalies of precipitation over China (Wang et al., 1994), displaying a circulation pattern similar to the well known "vortices with shear-lines mode" of Tao et al. (1980).

## 5. Acknowledgements

FUNDAÇÃO ORIENTE (Portugal) supported this research by offering Wang a scholarship for her Ph. D. study; Wang is grateful to Hohai University (P. R. China) for permitting her to study abroad. This research also benefited from the EC grant EV5V-CT92-0164 (project "Mediterranean Desertification and Land Use, Phase II"). We are very thankful to Mr. João Alves for his kind help in improving our diagrams. Professors Zhongxiu Fan, Enji Zhou and Gongbing Peng offered their warm-hearted help and strong encouragement to Wang on many aspects. Besides, the two reviewers provided constructive criticism and helpful suggestions.

## REFERENCES


Barnett, T. P. and Preisendorfer, R. W. 1978. Multifield analog prediction of short-term climate fluctuations using a climate state vector. *J. Atmos. Sci.* **35**, 1771–1787.

Barnston, A. G. and Livezey, R. E. 1987. Classification, seasonality and persistence of low-frequency atmospheric circulation patterns. *Mon. Wea. Rev.* **115**, 1083–1126.

Barrodale, I. and Erickson, R. E. 1980. Algorithms for least-squares linear prediction and maximum entropy spectral analysis, Part (I). Theory. *Geophysics* **45**, 420–432.

Branstator, G. 1992. The maintenance of low-frequency atmospheric anomalies. *J. Atmos. Sci.* **49**, 1924–1945.

Branstator, G. 1987. A striking example of the atmosphere's leading travelling pattern. *J. Atmos. Sci.* **44**, 2310–2323.

Corte-Real, J., Wang, X. and Zhang, X. 1995. Modes of variability in the northern hemisphere's mid-tropospheric large-scale circulation. *Theor. Appl. Climatol.* **50**, 113–146.

Hansen, A. R. 1993. A comparison between planetary-wave flow regimes and blocking. *Tellus* **45A**, 281–288.

Horel, J. D. 1981. A rotated principal component analysis of the interannual variability of the northern hemisphere 500 mb height field. *Mon. Wea. Rev.* **109**, 2080–2092.

Horel, J. D. 1984. Complex principal component analysis. Theory and examples. *J. Climate Appl. Meteor.* **23**, 1660–1673.

Kimoto, M. and Ghil, M. 1993a. Multiple flow regimes in the northern hemisphere winter. Part I. Methodology and hemispheric regimes. *J. Atmos. Sci.* **50**, 2625–2643.

Kimoto, M. and Ghil, M. 1993b. Multiple flow regimes in the northern hemisphere winter. Part II. Sectorial regimes and preferred transitions. *J. Atmos. Sci.* **50**, 2645–2673.

Lanzante, J. 1990. The leading modes of 10–30 day variability in the extratropics of the northern hemisphere during the cold season. *J. Atmos. Sci.* **47**, 2115–2140.

Legras, B., Desponts, T. and Piguet, B. 1987. Cluster analysis and weather regimes. In: *Proc. ECMWF Workshop on The nature and prediction of extra-tropical weather systems*, vol. 2. ECMWF, Reading, Shinfield Pk., UK.

Mo, K. C. and Ghil, M. 1987. Statistics and dynamics of persistent anomalies. *J. Atmos. Sci.* **44**, 877–901.

Mo, K. C. and Ghil, M. 1988. Cluster analysis of multiple planetary flow regimes. *J. Geophys. Res.* **93**, 10927–10951.

Molteni, F., Tibaldi, S. and Palmer, T. N. 1990. Regimes in the wintertime circulation over the northern extratropics. I. Observational evidence. *Quart. J. Roy. Meteor. Soc.* **116**, 31–67.

Plaut, G. and Vautard, R. 1994. Spells of low-frequency oscillations and weather regimes in the northern hemisphere. *J. Atmos. Sci.* **51**, 210–236.

Reinhold, B. B. and Pierrehumbert, R. T. 1982. Dynamics of weather regimes. Quasi-stationary waves and blocking. *Mon. Wea. Rev.* **110**, 1105–1145.

Tao, S. Y. et al. 1980. *Severe rainstorms over China.* Science Press, China. 225 pp. (in Chinese).

Thomson, D. J. 1982. Spectrum estimation and harmonic analysis. In: *Proceedings of the IEEE* **70**, 1055–1096.

Vautard, R. 1990. Multiple weather regimes over the north Atlantic. Analysis of precursors and successors. *Mon. Wea. Rev.* **118**, 2056–2081.

Vautard, R. and Legras, B. 1988. On the source of midlatitude low-frequency variability. Part II. Nonlinear equilibration of weather regimes. *J. Atmos. Sci.* **45**, 2845–2867.

Vautard, R., Yiou, P. and Ghil, M. 1992a. Singular-spectrum analysis: A toolkit for short, noisy chaotic signals. *Physica D* **58**, 95–126.

Vautard, R. and Plaut, G. 1992b. Low-frequency oscillations and weather regimes in the Northern Hemisphere. In: *Proc. ECMWF Workshop on Predictability* (European Centre for Medium Range Weather Forecasts, Reading, 1992).

Wallace, J. M. and Gutzler, D. S. 1981. Teleconnections in the geopotential height field during the northern hemisphere winter. *Mon. Wea. Rev.* **109**, 784–812.

Wang, X., Corte-Real, J. and Zhang, X. 1994. Large-scale circulation regimes and precipitation anomalies over China. *J. Meteor. Soc. Japan* **72**, 841–857.